Sciencexpress Report

Light-Controlled Self-Assembly of Semiconductor Nanoparticles into Twisted Ribbons

Sudhanshu Srivastava,[1] Aaron Santos,[1] Kevin Critchley,[1,2] Ki-Sub Kim,[1,3] Paul Podsiadlo,[1,4] Kai Sun,[5] Jaebeom Lee,[1,6] Chuanlai Xu,[1,7] G. Daniel Lilly,[1] Sharon C. Glotzer,[1]* Nicholas A. Kotov[1,5,6]*

[1]Department of Chemical Engineering, University of Michigan, Ann Arbor, MI 48109, USA. [2]School of Physics and Astronomy, University of Leeds, Leeds LS2 9JT, UK. [3]Department of Chemical and Biological Engineering, Chungju National University, 72 Daehak-ro, Chungju, Chungbuk 380-702, Republic of Korea. [4]Center for Nanoscale Materials, Argonne National Laboratory, Argonne, IL 60439, USA. [5]Department of Materials Science and Engineering and Department of Biomedical Engineering, University of Michigan, Ann Arbor, MI 48109, USA. [6]Department of Nanomedical Engineering, College of Nanoscience and Nanoengineering, Pusan National University, Miryang 627-706, Republic of Korea. [7]School of Food Science and Technology, Jiangnan University, Wuxi, Jiangsu 214122, China.

*To whom correspondence should be addressed. E-mail: sglotzer@umich.edu (S.C.G.); kotov@umich.edu (N.A.K.)

The collective properties of nanoparticles manifest in their ability to self-organize into complex microscale structures. Slow oxidation of Te^{2-} in CdTe nanoparticles results in the assembly of 1 to 4-μm long flat ribbons made of several layers of individual CdS/CdTe nanocrystals. Twisting of the ribbons with an equal distribution of left and right-helices was induced by illumination with visible light. The pitch lengths (250 to 1500 nanometers) varied with illumination dose, and the twisting was associated with the relief of mechanical shear stress in assembled ribbons caused by photooxidation of CdS. Unusual shapes of multiparticle assemblies, such as ellipsoidal clouds, dog-bone agglomerates, and ribbon bunches, were observed as intermediate stages. Computer simulations revealed that the balance between attraction and electrostatic repulsion determines the resulting geometry and dimensionality of nanoparticles assemblies.

Spirals, helicoids, helices, twisted ribbons (TRs), and other helical structures present fascinating geometries from the perspectives of mathematics, biology, optics, and mechanics. The formation of helices from nanoparticles (NPs) will make possible exploitation of the unusual properties of helices arising from quantum confinement (*1*, *2*) within NPs as well as expand the design space (*3*, *4*) and offer new means of controlling the pitch/chirality of the helical structures. In order to achieve self-organization of such intricate objects, it is necessary to fine tune the overall balance of forces including anisotropy of interactions that drive assembly of NPs into larger structures. Control of these processes will require the discovery of many-body interactions at the nanoscale, as well as understanding their dynamics and capabilities of formation of complex self-organized patterns transitioning from nano- to micro-scale.

As a model system for realizing these goals, an aqueous dispersion of CdTe (*5*) NPs (emission maximum at 550 nm) prepared (*6*) using thioglycolic acid (TGA) as a stabilizer with the TGA to Cd^{2+} ratio close to ~1.0, rather than the traditional value of 2.4 (*7*). Based on variety of existing data (*1*, *6*, *8*), these NPs exhibit strong anisotropy due to permanent dipoles on them (*1*, *8*). The strongly reduced concentration of TGA is expected to lead to the elimination of tetrahedral apices, where the local concentration of TGA is the highest and increase of the average value of dipole on NPs. It also increases chemical reactivity of the NPs, which intricately interplays with the interparticle forces. After preparation, the CdTe NPs are precipitated by addition of methanol and centrifuged for 20 min followed by redispersion in deionized water at pH = 9 (adjusted by addition of NaOH). The orange color of the NP solution turns dark green within ~72 hours, indicating that NP self-assembly has occurred.

Twisted ribbons (TRs) with distinctive helicity (Fig. 1, A, B, and D to F), were the primary product of the aging process (Fig. 1) (*6*) The length of the TRs made from CdTe typically ranged from 0.8 to 2 μm, but can be as long as 8 μm (Fig. 1). Some of straight nanowires (NWs) were also produced as a secondary product (Fig. 1C) and were identified as well-studied single crystalline Te wires (*7*) (fig. S1). Unlike these NWs or other NP assemblies (*6*), the TRs were made from individual NPs layered on top of each other (Fig. 1, G to I). Their thickness,. As determined by atomic force microscopy (AFM), was 10 to 12 nm and corresponds to 3-4 NP layers. The pitch of the CdTe TRs averaged ca. 350 nm (Fig. 1, E and F). The distribution between right- and left-handed twisting was approximately equal: 52% right: 48% left, which indicates a nearly racemic mixture of chiral isomers (*7*) (fig. S2). Remarkably, the helical ribbons form bundles in which all TRs have the same chirality. Instead of the typical red shift

of optical features found in previous studies of NP assemblies (*6*, *9*, *10*), a gradual blue shift of the luminescence and absorption peaks was observed during formation of TRs (Fig. 2A). This observation normally would have indicated the decrease in delocalization volume of excitons in CdTe and, hence, a wholly different process is taking place than previously reported. This phenomenon is rather unusual but can be understood when the entire process of transformation of NPs to helicoidal structures is discussed.

We first characterized the composition of the products with x-ray energy dispersive spectroscopy (XEDS). The atomic% Cd:Te:S ratio for TRs and original CdTe NPs was 46:10:44 and 43:38:19, respectively. The assembly process is associated with considerable loss of Te and transition to CdS/CdTe NPs in which CdS phase is strongly dominant. This substantial change of the composition can be observed in high-resolution transmission electron microscopy images (HRTEM, Fig. 2, C and D). The lattice spacings for {111} planes for as-prepared CdTe NPs is 0.384 nm, but is shorter for NPs in TRs, 0.344 nm (Fig. 2C) as expected for CdS particles. Selected-area electron diffraction (SAED) patterns of the TRs showed the presence of characteristic diffraction patterns for both CdTe (111) (d = 0.38 nm), (220) (d = 0.22 nm) and CdS (100) (d = 0.34 nm), (110) (d = 0.31 nm) (101) (d = 0.19 nm) planes (*11*) (Fig. 2, E and F). These data and the presence of Te NWs indicate that the process of oxidation Te^{2-} to Te^{0} takes place.

To gain better knowledge about the transformation of NPs into TR, dynamics of multiparticle assembly, and driving forces of this process, we investigated the intermediate stages of particle self-organization with corresponding trends in atomic composition. Both CdTe and CdS are light sensitive (*12*) so subsequent studies were carried out both in dark and light conditions.

Examination of 1, 12, 24, and 72 hours time points of samples assembled under ambient light by scanning electron microscopy (SEM) and TEM revealed an interesting evolution of shapes of the multiparticle assemblies. Small spherical agglomerates were the starting point of NP->TR transition and were exclusively present at 1 hour time point after re-dispersion. By 12 hours they transformed into much larger spheroids with complex elongated shape (Fig. 3A) and then evolved into dog-bone shaped NP systems by 24 hours (Fig. 3B). In 48 hours from the beginning of the self-assembly process, the dog-bone agglomerates reorganized themselves by stretching along a specific axis resulting in fairly thick NWs (Fig. 3C) (*13*). At 72 hours, the thicker linear assemblies lead to thinner ones. Upon closer examination they were the bunches of NWs or ribbons which unravel as “bouquets” of TRs of the same chirality (*7*) (Fig. 3D and fig. S2). Note that the transition of spherical agglomerates to dog-bone shaped assemblies is associated with drastic reduction of Te contents, which subsequently increased only slightly.

When the concentration of NPs was reduced from the beginning of the reaction, dog-bone stage disappeared, individual nanoribbons were formed as an intermediate stage, and the TRs emerged at ~24 hours, followed by their bundling together at 72 hours (*7*) (fig. S4). These results indicated that ribbons represent an important intermediate product of NP-TR transition regardless whether they are individual or associated into bunches.

When assembly takes place in the dark, after 1 hour, the NPs form loosely associated agglomerates that, again, exhibit a tendency to consolidate (Fig. 3E) by 12 hours. No intermediate dog-bone shaped structures were observed. Indeed, their presence must be associated with large number of stronger interacting particles. Instead, the NPs transformed into straight, multiparticle ribbons in 24 hours, which were also bunched together (Fig. 3F). These ribbons exhibited the propensity to debundle and become thinner after 48 hours (Fig. 3G). Eventually, the reaction in the dark resulted in distinct long straight ribbons (Fig. 3H) in 72 hours with no twisting, which confirmed the importance of (*1*) straight ribbons as an intermediate stage and (*2*) light for NP->TR transition. It also offered a new means of control over helical NP assemblies.

XEDS data (*7*) (Fig. 3, A to H, and fig. S6) for all the complex intermediate stages in both light and dark conditions reveal important points about the nature of the processes taking place and origin of the unusual twisted morphology. The oxidation of Te^{2-} takes place both in light and in dark. After 24 hours, *i.e.* at the dog-bone stage for light and bunched nanoribbons stage for dark conditions, the NPs are made predominantly made from CdS with only 3-5% of Te atoms. The amount of S in illuminated samples is consistently lower than that in NPs made in dark, and photocorrosion of CdS must be associated with the appearance of the twisted geometry. The conclusion can also be confirmed by larger {111} lattice spacing observed in the assemblies obtained in light than in dark conditions (*7*) (fig. S13). Photooxidation of Te^{2-} leads to the strong change of chemical make-up of the NPs, accompanies the general assembly in ribbons, but it alone cannot be responsible for the appearance of helical assemblies.

The photooxidation of CdS in CdS/CdTe nanoparticles before the complete removal of Te^{2-} centers may seem counterintuitive. However, the particles assembling into the ribbons and undergoing the twisting process, are primarily made from CdS already (97-95%). The preference for oxidation of CdS over CdTe originates most likely from the gradient core-shell structure of the NPs obtained by replacement of Te with S during Te^{2-} oxidation stage (*7*). SAED pattern indicate the presence of both CdTe and CdS

phases (Fig. 1F), which is consistent with core-shell morphology. The surface of the NPs is likely to be pure CdS, while the Te atoms concentrated in the core become shielded from the photoreaction with dissolved oxygen. Also note that the areas of delocalization of hole and electron tend to separate in NPs with CdTe/CdS heterojunctions, which increases the probability of interfacial photocorrosion.

We further explored the effects of illumination on NP->TR transitions. As such, TRs (~50 nm wide) prepared under 61 μW (ambient), 45, 38, and 21 μW, showed a pitch length of ~250-400 (Fig. 3I), ~500-600 nm, ~1000 nm and ~1500 nm (Fig. 3J), respectively (*7*) (fig. S7). At all light intensities, HRTEM demonstrated the same polycrystalline nature composed of CdTe/CdS NPs. The dependence of the pitch length of TRs on light can also be traced in the dose of photons. A sample was aged in dark for more than 2 days to form straight ribbons (Fig. 3K) and then was illuminated by ambient light (61 μW). The SEM images showed sequential change the pitch length was ~400 nm pitch length after 24 hours in light, respectively (Fig. 3L).

The series of transformations of NPs and subsequent structures observed are different from the reactions reported in previous organic or inorganic helical systems (*14*) or other NP assemblies (*15*, *16*). This necessitates gaining further insight into the balance of forces behind the TR formation. Typical helical structures originate from either specific crystal lattice distortions (*17*), mechanical strains (*18*), or chiral building blocks, and form directly from the constituents. Helical structures can be formed because of mechanical stress or mismatch of the crystal lattice planes. The truncated tetrahedral structures of cubic II-VI semiconductor NPs can potentially be chiral, but we obtained no experimental evidence for chirality of individual NP involved in the NP->TR transition. The polycrystalline nature and the existence of two distinct crystalline phases: CdTe and CdS, in the TRs, made the possibility of oriented attachment (*19*) and screw axis dislocations (*20*) in the extended crystal lattice as sources of helicity are highly unlikely. Moreover, both of these mechanisms of helix formation at the nanoscale typically result in much shorter (by one to two orders of magnitude) pitch lengths than those observed in Fig. 1.

We propose the following model for TR formation. Initially, between 1 and 24 hours, in both light and dark conditions, the attraction between the NPs is relatively weak and dynamic aggregates with fairly spherical shape are produced (Fig. 3, A and E). The same period of time overlaps with completion of Te replacement with CdS. This change to CdS-dominant NPs prevents them from recrystallization into CdTe thin cylindrical NWs seen before (*6*), because CdS has greater activation barrier of recrystallization (*6*).
The forces between NPs are substantially stronger for light conditions and the spheroids are larger and denser (Fig. 3A) than in dark. We hypothesize that the multiparticle spheroids evolve into the dog-bone shaped structures (Fig. 3B) because of gradual increase of anisotropic dipolar NP-NP interactions and the tendency of electric dipoles to align (*6*). The thin center part of the dog-bone and its conical apexes pointing to each other from each "pole" form through NP reorganization caused by forces that favor axial distribution. The potential origins of the greater dipolar interactions in the illuminated NPs are the entrapment of photogenerated charges at the interfacial states and unequal photoetching, which increases the value of the dipole moment (*21*). The reorganization continues until the round "clouds" become separated and eventually reorganize by stretching, producing ribbons and their bundles (Fig. 3, C and D).

Unlike the initial round agglomerates, the layers of NPs in the ribbons are well connected to each other (Fig. 2B) by short-range van der Waals interactions, hydrophilic/hydrophobic, dipole-dipole and charge-dipole forces. In such objects twisting can be produced as a result of internal shear strain between different NP layers, which can be partially relieved by acquiring the helical shape with uniform pitch length despite some increase of elastic energy stored in the ribbon as a whole upon twisting. This is a common property of many ribbon-like structures (*22*) and was also observed in ribbons from multiwalled carbon nanotubes which acquire twisted conformation to gain better registry between interacting graphene sheets (*23*). The source of internal strain in our ribbons is light-induced photocorrosion (*24*, *25*) of individual NP units, which results in reorganization of the bonded NPs trying to attain better/different packing due to the change of charge and/or dipole moment.

In the dark, no strain is generated, and the ribbons remain straight (Fig. 3, H and K) but tend to bunch. When light is on, photocorrosion of CdS results in the increase of charge/dipole in the already assembled ribbons, the stress between the layers of NPs gradually builds up with increasing the time or intensity of illumination and twisting occurs. A greater degree of photoetching results in greater strain in the ribbons, and hence stronger twisting (Fig. 3, I and J). The overall dose of illumination is most important in this respect, and hence the twisting can be controlled by both intensity (Fig. 3, I and J) and the time of light exposure (Fig. 3L).

Different experimental results, such as TEM/SEM images, XEDS, x-ray photoelectron spectroscopy (XPS) and dynamic light scattering data (*7*) (Figs. 1 to 3) match this mechanism of NP assembly into TRs very well. Changes in atomic% composition seen in XEDS (*7*) (Fig. 3, A to H, and fig. S6) and XPS data (*7*) (figs. S8 to S11) confirmed photoinduced oxidation of CdS. There are two additional pieces of evidence for this mechanism, which are particularly revealing. The key role of oxidation in TRs formation can be confirmed by

performing the NP self-organization reaction in under inert atmosphere. Even under light, no twisting was observed (*7*) (fig. S12), when oxygen was excluded from the reaction. As well, the steady increase of zeta-potential of NPs (fig. S15) from -10 mV to -50 mV clearly indicated that photoreaction results in great increase of particle charge. This finding confirms generation of a strong long-distance strain in the ribbons upon illumination. Alternatively, chemical oxidation with H_2O_2 fails to generate high zeta potential (always below -25 mV and eventually drops to zero) and hence fails to produce TRs (*7*) (fig. S18).

To further understand the assembly process, we carried out computer simulations to ascertain why the NPs under these conditions produce ribbons as the key precursors to TRs in light and dark conditions, and not chains (*8*) or sheets (*1*) as previously found for the same NPs under different conditions. This is also important from the perspective of understanding and controlling the forces between the NPs, so that the design of twisted and other self-organized microstructures can be done at the NP level. To describe self-organization process of NPs, we used the same coarse-grained simulation model as Zhang *et al*. (*1*, *8*, *26*) with modified parameters (*7*) to account for the present experimental conditions. Our choice of parameters reflects the reduced amount of TGA per CdTe resulting in a net decrease of the charge, and an increase of the face-face attraction energy, and a change in the direction of the dipole moment as compared to the conditions under which chains are obtained.

We used a recently developed technique for predicting ordered assemblies of building blocks with strong interactions, bottom-up building block assembly (BUBBA) (*27*), to determine the preferred local packing structure of tetrahedrons within ribbons. Then Monte-Carlo simulations were used to calculate the energy as a function of ribbon width to ascertain whether, and under what conditions, ribbons of finite width (rather than chains or sheets) (*1*, *8*) were the minimum energy structures. We found that NPs form bilayers with tetrahedrons arranged hexagonally and inverted in alternate layers for denser packing (Fig. 4), which is consistent with TEM and SEM observations (Fig. 2B) albeit without the packing perfection seen in the simulations. The energy of the ribbon is minimized for a range of widths of ~18-110 nm, which matches structural parameters of TRs (Figs. 1 to 3) very well. Increasing the charge resulted in more narrow ribbons, while decreasing the charge resulted in wider ribbons.

Overall, the multiparticle behavior and transition from packing into chains, ribbons, and sheets, can be understood in terms of a competition between the face-face attraction and the charge-charge repulsion. For low charge and strong face attraction as was the case in previous study (*1*, *8*), particles pack very densely and would, if constrained to the same packing structure, form infinite two-dimensional sheets. By increasing the amount of charge, infinite plane becomes energetically unfavorable because of the long-range electrostatic repulsion, and NPs assemble as ribbons. Further increase of particle charge will eventually result in chains, as was indeed observed for higher concentration of TGA (*6*). Note that this concerns the effect of NP charge before the assembly. Once a larger NP system is assembled and held together by strong interparticle interactions, it may not be able to transition freely from sheets to ribbons of smaller width and then to chains. However, if there are structural units more loosely attached to each other, such as ribbons in bunches, they do separate as can be seen by the unraveling of the "bouquets" of TRs (Fig. 3D and fig. S14).

The notion of evolving NP assemblies and better understanding of parameters controlling behavior of large numbers of nanoscale particles as a whole will be useful for many other nanocolloid systems. The modulation in the pitch length for the TRs under different light intensities, creates a new approach in the synthesis of nanostructures and new opportunities to generate novel nanomaterials with controlled circular dichroism and other optical, electronic, and mechanical properties.

References and Notes

1. Z. Tang, Z. Zhang, Y. Wang, S. C. Glotzer, N. A. Kotov, *Science* **314**, 274 (2006).
2. R. S. Yang, Z. L. Wang, *J. Am. Chem. Soc.* **128**, 1466 (2006).
3. S. C. Glotzer, M. J. Solomon, N. A. Kotov, *AIChE J.* **50**, 2978 (2004).
4. S. C. Glotzer, M. J. Solomon, *Nat. Mater.* **6**, 557 (2007).
5. C. Li, N. Murase, *Chem. Lett.* **34**, 92 (2005).
6. Z. Tang, N. A. Kotov, M. Giersig, *Science* **297**, 237 (2002).
7. See supporting material on *Science* Online.
8. Z. Zhang, Z. Tang, N. A. Kotov, S. C. Glotzer, *Nano Lett.* **7**, 1670 (2007).
9. W. W. Yu, L. H. Qu, W. Z. Guo, X. G. Peng, *Chem. Mater.* **15**, 2854 (2003).
10. J. Guo, W. Yang, C. Wang, *J. Phys. Chem. B* **109**, 17467 (2005).
11. K. V. K. Rao, S. V. N. Naidu, L. Iyengar, *J. Am. Ceram. Soc.* **51**, 467 (1968).
12. M. T. S. Nair, P. K. Nair, R. A. Zingaro, E. A. Meyers, *J. Appl. Phys.* **75**, 1557 (1994).
13. S. Busch *et al*., *Eur. J. Inorg. Chem.* **1999**, 1643 (1999).
14. M. J. Bierman, Y. K. A. Lau, A. V. Kvit, A. L. Schmitt, S. Jin, *Science* **320**, 1060 (2008).
15. Y. Zhou, Q. M. Ji, M. Masuda, S. Kamiya, T. Shimizu, *Chem. Mater.* **18**, 403 (2006).
16. T. Vossmeyer *et al*., *Science* **267**, 1476 (1995).

17. K. S. Cho, D. V. Talapin, W. Gaschler, C. B. Murray, *J. Am. Chem. Soc.* **127**, 7140 (2005).
18. L. S. Li, H. Z. Jiang, B. W. Messmore, S. R. Bull, S. I. Stupp, *Angew. Chem. Int. Ed.* **46**, 5873 (2007).
19. D. V. Talapin, H. Yu, E. V. Shevchenko, A. Lobo, C. B. Murray, *J. Phys. Chem. C* **111**, 14049 (2007).
20. X. D. Han *et al*., *Nano Lett.* **7**, 452 (2007).
21. Y. Wang, Z. Tang, M. A. Correa-Duarte, L. M. Liz-Marzán, N. A. Kotov, *J. Am. Chem. Soc.* **125**, 2830 (2003).
22. T. McMillen, A. Goriely, *J. Nonlinear Sci. E* **12**, 241 (2002).
23. M.-F. Yu *et al*., *Phys. Rev. B* **64**, 241403 (2001).
24. S. Yang *et al*., *J. Am. Chem. Soc.* **128**, 10460 (2006).
25. A. Goriely, P. Shipman, *Phys. Rev. E* **61**, 4508 (2000).
26. G. D. Phillies, *J. Chem. Phys.* **60**, 2721 (1974).
27. D.-J. Hong *et al*., *Angew. Chem.* **48**, 1664 (2009).
28. The authors acknowledge joint financial support by the Air Force Office of Scientific Research under MURI grant FA9550-06-1-0337. P.P. thanks the Fannie and John Hertz Foundation for support of his work through a graduate fellowship. This research was supported by WCU (World Class University) program through the Korea Science and Engineering Foundation (KOSEF) funded by the Ministry of Education, Science and Technology (MEST, R33-2008-000-10021-0). The authors thank Prof. Jinsang Kim (University of Michigan) for helpful suggestions and discussions. The authors thank Dr. Wei Chen (JiangNan University) for assistance with some TEM data. P.P.'s work at the Center for Nanoscale Materials was supported by the Office of Science, Office of Basic Energy Sciences, of the U.S. Department of Energy under contract no. DE-AC02-06CH11357. P.P. acknowledges the support of Willard Frank Libby postdoctoral fellowship from Argonne National Laboratory. The TEM used in the study was supported by NSF grant DMR-9871177 and the SEM used was supported by NSF grant DMR-0320740.

Supporting Online Material

www.sciencemag.org/cgi/content/full/science.1177218/DC1
Materials and Methods
SOM Text
Figs. S1 to S22
References

3 June 2009; accepted 2 February 2010
Published online 11 February 2010; 10.1124/science.1177218
Include this information when citing this paper.

Fig. 1. (**A** and **B**) SEM (A) and TEM (B) images of bundles of TRs. (**C** and **D**) Individual straight Te NWs (C) and CdTe/CdS TRs (D). (**E** and **F**) SEM (E) and atomic force microscopy (AFM) images (F) of individual TRs with pitch lengths of 380 nm (E) and 400 nm (F). (**G**) TEM image of a crosssection of TRs (the cutting plane may not be perpendicular to the TR axis). (**H** and **I**) AFM image and AFM crosssectional analysis of TRs.

Fig. 2. (**A**) Evolution of fluorescence spectra for the self-organization of NPs into TRs. (**B**) HRTEM images for CdTe TRs taken in the "twist region". (**C** and **D**) Lattice fringes for {111} planes for the as-prepared NPs (C) and those in TR (D). (**E** and **F**) SAED patterns from CdTe NPs (E) and TR (F) with diffraction rings characterizing CdTe and CdS marked in red and yellow, respectively.

Fig. 3. Intermediate stages of TR formation and control of the twisting pitch. (**A** to **H**) SEM images of the ribbons assembled in ambient light (A) 12 hours, (B) 24 hours, (C) 48 hours, (D) 72 hours after redispersion of stabilizer depleted particles and the ribbons assembled in dark at the same time points: (E) 12 hours, (F) 24 hours, (G) 48 hours, (H) 72 hours. The XEDS Cd:Te:S atomic ratios for the particle assemblies are given below the corresponding images. (**I** and **J**) TRs prepared at different light intensities: (I) 61 μW, and (J) 21 μW. (**K** and **L**) SEM images of ribbons after 52 hours in dark assembly (K) and then (L) illuminated by the ambient light (61μW) for 24 hours. NP concentration 5 μM.

Fig. 4. (**A**) A truncated tetrahedron particle used in the simulations. (**B**) Close up of the hexagonal packing structure obtained from BUBBA. (**C**) Plot of the per particle energy measured in kJ/mol versus the width of a ribbon measured in particles. (**D** and **E**) Top and side views of straight ribbons, respectively. Pink and yellow tetrahedra point up; green and red tetrahedra point down.

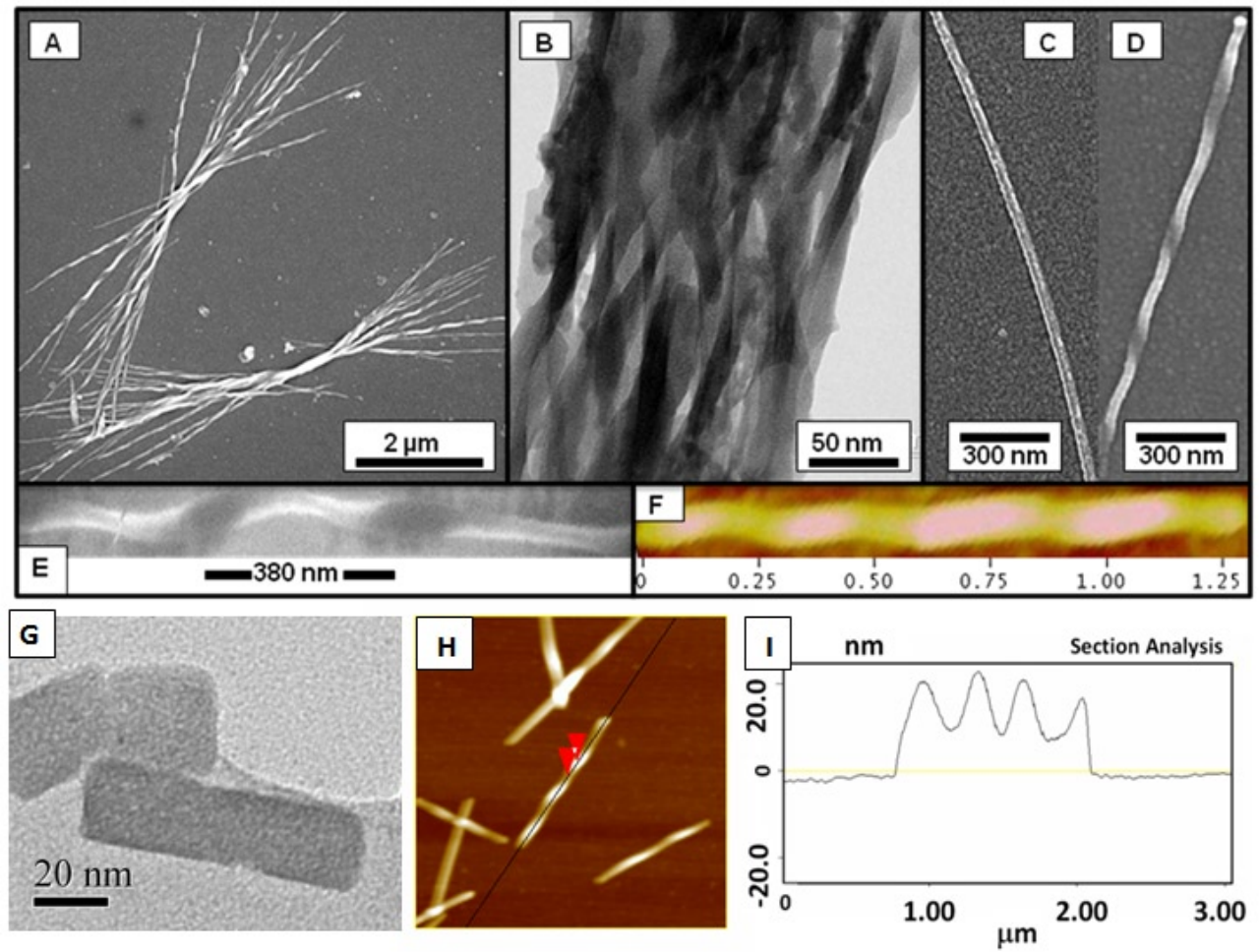
A
2 µm
B
50 nm
C
300 nm
D
300 nm
E
380 nm
F
0
0.25
0.50
0.75
1.00
1.25
G
20 nm
H
I
nm
Section Analysis
20.0
0
-20.0
0
1.00
2.00
3.00
µm

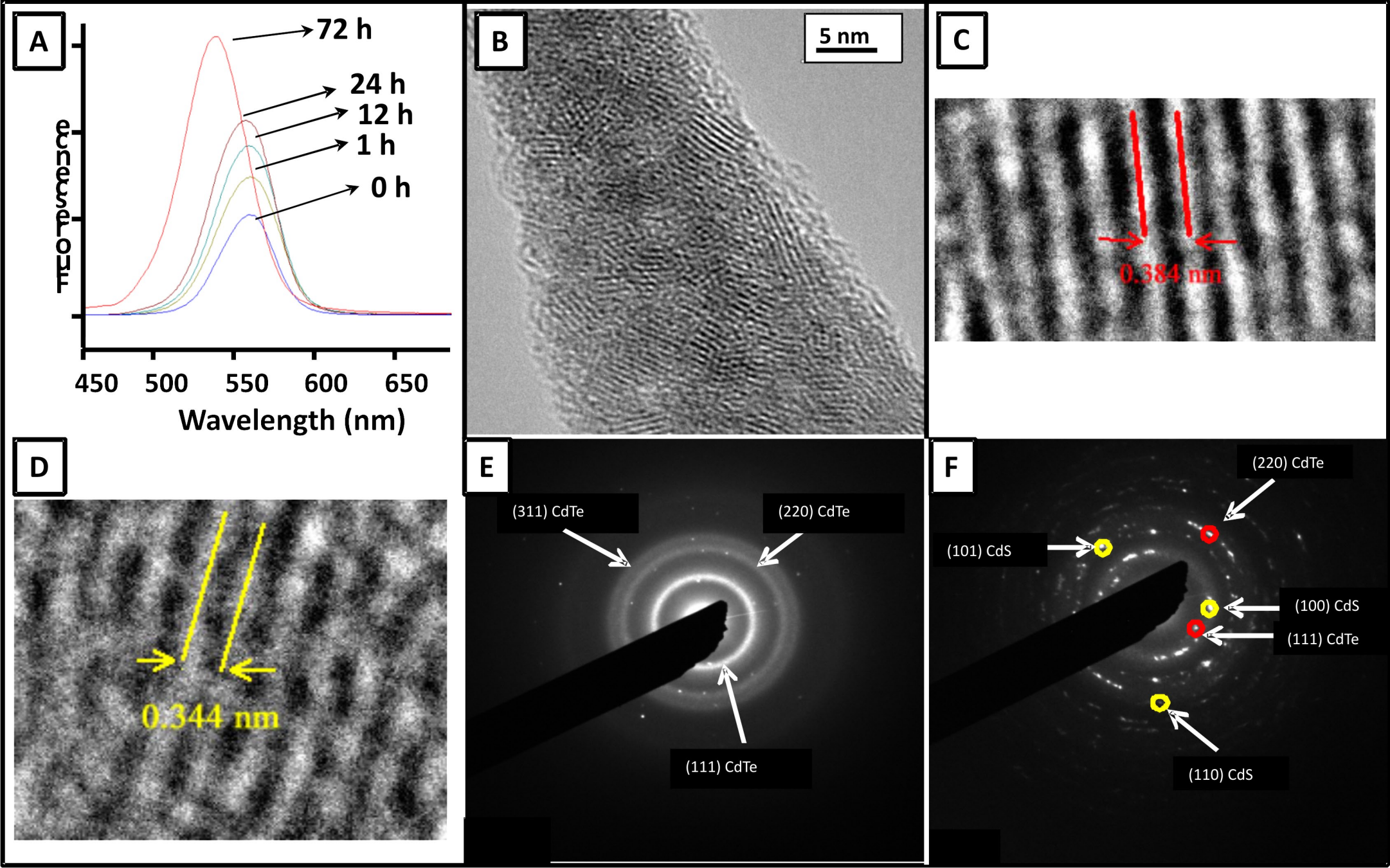
A
72 h
24 h
12 h
1 h
0 h
Intensity
450
500
550
600
650
Wavelength (nm)
B
5 nm
C
0.384 nm
D
0.344 nm
E
(311) CdTe
(220) CdTe
(111) CdTe
F
(220) CdTe
(101) CdS
(100) CdS
(111) CdTe
(110) CdS

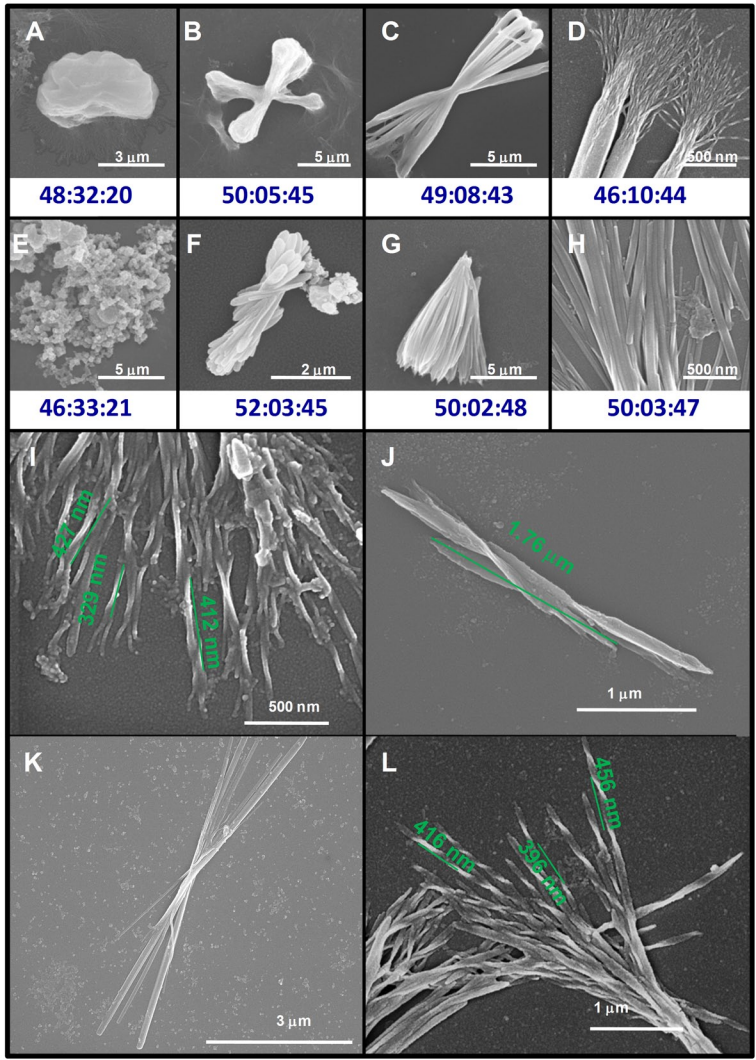
A
3 μm
B
5 μm
C
5 μm
D
500 nm
48:32:20
50:05:45
49:08:43
46:10:44
E
5 μm
F
2 μm
G
5 μm
H
500 nm
46:33:21
52:03:45
50:02:48
50:03:47
I
424 nm
328 nm
412 nm
500 nm
J
1.76 μm
1 μm
K
3 μm
L
456 nm
416 nm
396 nm
1 μm

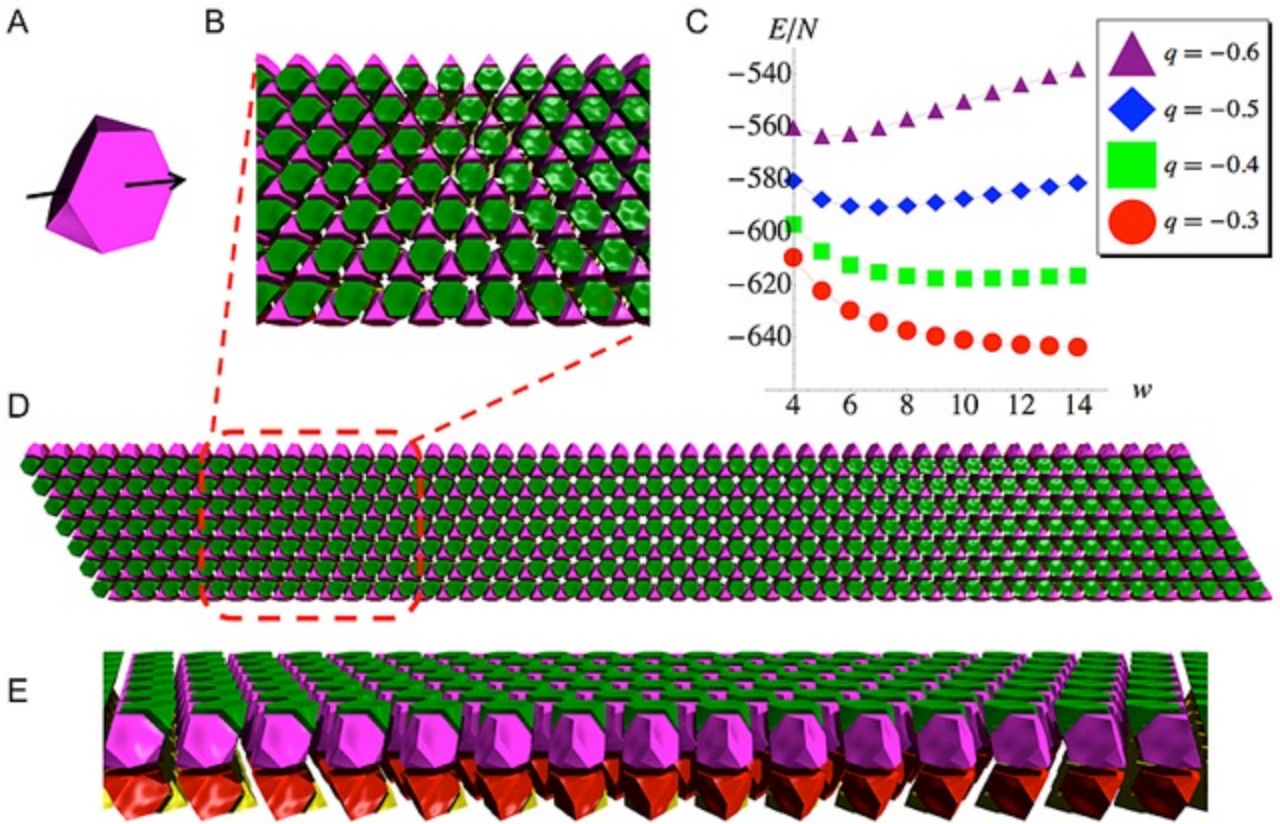
A
B
C
E/N
−540
−560
−580
−600
−620
−640
4
6
8
10
12
14
w
q = −0.6
q = −0.5
q = −0.4
q = −0.3
D
E